Probing the coordination environment of Ti³⁺ ions coordinated to nitrogen-containing Lewis bases

Morra, E.; Maurelli, S.; Chiesa, M.; Van Doorslaer, S.. Probing the coordination environment of Ti^{3+} ions coordinated to nitrogen-containing Lewis bases. PHYSICAL CHEMISTRY CHEMICAL PHYSICS. 17 (32) pp: 20853-20860.
DOI: 10.1039/c5cp03417e

Probing the Coordination Environment of Ti^{3+} Ions Coordinated to Nitrogen Containing Lewis Bases

E. Morra,[abc] S. Maurelli,[a] M. Chiesa,*[a] S. Van Doorslaer*[b]

Multi-frequency continuous-wave and pulse EPR techniques are employed to investigate the coordination of nitrogen-containing ligands to Ti^{3+}-chloro complexes. Frozen solutions of $TiCl_3$ and $TiCl_3(Py)_3$ dissolved in nitrogen-containing solvents have been investigated together with the $TiCl_3(Py)_3$ solid-state complex. For these different systems, the hyperfine and nuclear quadrupole data of Ti^{3+}-bound ^{14}N nuclei are reported and discussed in the light of DFT computations, allowing for a detailed description of the microscopic structure of these systems.

Introduction

Titanium (III) compounds play an important role in both homogeneous and heterogeneous catalysis in the fields of olefins polymerization[1,2] and hydrogenation[3] or as initiators in radical reactions.[4]
Catalytically active species are characterized by specific oxidation states and coordination geometries, which ultimately determine the activity and (stereo)selectivity of the catalyst. The link between the catalytic activity and molecular geometry emphasizes that a profound knowledge of the electronic and geometrical structure of the active site, at the molecular level, is of fundamental importance in understanding and designing highly active catalysts. Hence, synthetic factors that provoke any, even subtle, modifications to the nature of the active site deserve a thorough study. The nature of the ligands is of outmost importance in modulating the chemical and catalytic potential as well as the selectivity of transition-metal ion complexes in both homogeneous and heterogeneous systems. In the case of Ti^{3+} many of the relevant complexes active as homogeneous and heterogeneous catalysts feature nitrogen-containing ligands. In the current work, we investigate by means of multi-frequency continuous-wave (CW) and pulse EPR the coordination of titanium (III) ions to nitrogen-containing Lewis bases, which are important electron donors in high-yield Ziegler-Natta catalysts. These catalysts are heterogeneous systems, which owe their formidable activity and selectivity to the complex relationships between a crystalline $MgCl_2$ matrix, the $TiCl_4$-active phase and the presence of electron-donor adsorbates, whose role in determining the stereoselectivity of the polymerization is still nowadays not fully understood.
We recently demonstrated that advanced EPR experiments can shed light on the nature of potentially Ti^{3+} active sites in heterogeneous Ziegler-Natta catalysts, providing insights into their local geometry and environment.[5] In order to interpret the complex spectra associated with the heterogeneous catalyst, however, reliable reference data are needed, which can be obtained from model systems. Recently, we have investigated the spectroscopic properties of $TiCl_3$ dissolved in methanol solutions[6] elucidating the geometric and electronic structure of the formed molecular complexes, obtaining the full set of spin Hamiltonian parameters for coordinated chlorine and methanol or OH^- groups. In an effort to extend the set of reference data to nitrogen-based ligands, we studied frozen solutions of Ti^{3+} chloride dissolved in 1-methyl imidazole and in pyridine and the solid-state compound $TiCl_3(Py)_3$. In this way a detailed characterization of paramagnetic Ti^{3+} in different systems containing directly coordinated nitrogen ligands has been achieved and a detailed description of the microscopic structure obtained by comparison of the experimental data with DFT-computed parameters.

Experimental and computational details

Ti^{3+} solutions were prepared in a glove-box under controlled atmosphere (oxygen content < 3ppm_V, water content < 2.5 ppm_V). The violet α-polymorph of $TiCl_3$ (α-$TiCl_3$) was dissolved in anhydrous 1-methyl imidazole, while the green $TiCl_3(Py)_3$ complex was dissolved in pyridine. For both systems, solutions at different concentrations were prepared. In particular the results obtained for solutions of concentration [C] ≈ 0.2 M (hereafter referred to as concentrated) and [C] ≈ 0.02 M (hereafter referred to as diluted) will be discussed. The colour of the methylimidazole solutions are purple (concentrated) and green (diluted) respectively, while the pyridine solutions have a red colour. The α-$TiCl_3$ and the $TiCl_3(Py)_3$ complex were kindly provided by Prof. M. Terano, (JAIST, Japan).

Spectroscopic details

CW and pulse X- and Q-band EPR experiments were performed on a Bruker Elexsys E580 spectrometer, operating at a microwave frequency of 9.76 GHz and 34 GHz. W-band EPR measurements were performed on a Bruker E680 spectrometer, operating at 94 GHz. The EPR spectrometers are equipped with helium gas-flow cryostats (Oxford, Inc.). The X-band CW-EPR measurements were performed with a microwave (mw) power of 0.015 mW, a modulation frequency of 100 kHz and modulation amplitude of 0.5 mT. For the W-band CW-EPR measurements mw power 1.39 μW and modulation frequency 100 kHz were used.

Electron spin echo (ESE) detected EPR experiments were carried out with the pulse sequence: $\pi/2-\tau-\pi-\tau-$echo. At X-band, the mw pulse lengths $t_{\pi/2}$ = 16 ns and t_{π} = 32 ns and a τ value of 200 ns were used. Q-band conditions were as follows: $t_{\pi/2}$ = 16 ns and t_{π} = 32 ns and a τ value of 300 ns. W-band conditions were $t_{\pi/2}$ = 100 ns and t_{π} = 200 ns and a τ= 600 ns. A 1 kHz repetition rate was used at all mw frequencies.

Hyperfine Sublevel Correlation (HYSCORE)[7] experiments were carried out with the pulse sequence $\pi/2-\tau-\pi/2-t_1-\pi-t_2-\pi/2-\tau-$*echo*. The time traces of the HYSCORE spectra were baseline corrected with a third-order polynomial, apodized with a Hamming window and zero-filled. After two-dimensional Fourier transformation, the absolute value spectra were calculated. A shot repetition rate of 1.25 kHz was used at both X- and Q-band frequencies. A four-step phase cycle (for X-band experiments) or an eight-step phase cycle (for Q-band experiments) was used to remove unwanted echoes.

ELDOR-detected NMR (EDNMR)[8] measurements were performed at the W-band frequency using the pulse sequence HTA–$T-\pi/2-\tau-\pi-\tau-$*echo*. The high turning angle (HTA) microwave pulse was applied at microwave frequency ν_2. The detection Hahn echo pulse sequence $\pi/2-\tau-\pi-\tau-$*echo* was matched to the cavity resonance microwave frequency ν_1 and the spectra were acquired via continuously sweeping the HTA frequency ν_2 at fixed B_0. After symmetrization of left and right side, the experimental spectrum was phase corrected and inverted. The central blind spot was subtracted considering a lorentzian fit. The experimental settings employed are t_{HTA}= 5000 ns, $t_{\pi/2}$= 120 ns, delay between the HTA pulse and the detection sequence T=500ns. The spectrum was acquired with 12 scans.

All of the EPR spectra were simulated using the Easyspin[9] package.

Computational details

Spin-Hamiltonian parameters were calculated for different Ti^{3+} model complexes using spin-unrestricted density functional computations with the ORCA computational package.[10] Geometry optimizations were performed using the BP86 functional[11] with the triple polarized core-properties CP(PPP)[12] basis set for Ti, the polarized triple-ζ valence TZV(PP)[13] basis set for Cl and SVP basis set for all other atoms. The computations of the EPR data were performed using the PBE0 functional in combination with the CP(PPP) basis set for Ti, the TZV(PP) basis set for Cl and EPR-II[14] for all other atoms. This level of theory was validated by previous studies on similar compounds.[6,15] The solvent surrounding was simulated using the COSMO model.[16]

Results and discussion

EPR and HYSCORE experiments

Dissolving $TiCl_3$ in 1-methyl imidazole leads to characteristic EPR spectra whose features are dependent on the Ti(III) concentration. In Figure 1 representative CW and ESE-detected EPR spectra recorded at X- and W-band frequencies are shown for two different concentrations differing approximately by an order of magnitude ([C] ≈ 0.2 M – 0.02 M). In both cases the X-band CW EPR spectra (Figure 1c and 1g) are dominated by a signal with low anisotropy centered at g≈1.96. More resolved spectra are obtained at W-band frequency, where in the case of the more concentrated solution an additional broad absorption feature is clearly observed in the 3400-3800 mT region (Figure 1d). Given the broad line width of this second signal a better resolved spectrum is obtained by recording the ESE-detected EPR spectrum, which measures the absorption signal directly (Figure 1b). In this case both X- and W-band ESE-detected EPR spectra (Figures 1a and 1b) of the concentrated solution show clearly the presence of a relatively broad and anisotropic signal at higher field, which is absent in the diluted solution. The overall spectrum can be rationalized in terms of the superposition of three species (referred to as monomers 1-3), whose spin-Hamiltonian parameters have been obtained by computer simulation (Table 1). In particular the broad and anisotropic high-field portion of the spectrum can be simulated considering two centres (monomers 2 and 3 in Table 1). The linewidth is relatively broad and this can be explained considering strain effects induced by a plurality of slightly differing solvation structures and/or by ^{47,49}Ti hyperfine interactions. The measured g values and the overall spectral shape agree with data previously obtained by us for $TiCl_3$ dissolved in methanol solutions.[6] The third species (monomer 1) dominates the spectrum of the diluted solution (Figure 1e-h) and can be simulated with a nearly isotropic $\boldsymbol{g}$ tensor. Previous works report a marked decrease of the $\boldsymbol{g}$ tensor anisotropy upon treatment of Ti molecular complexes and $MgCl_2$-supported systems with an N-containing solvent, *i.e.* pyridine, which is associated to the formation of $TiCl_3$·nPy adducts.[17,18] This is consistent with the observed reduction of the $\boldsymbol{g}$ anisotropy for the diluted $TiCl_3$ solution in 1-methyl imidazole.

In the X-band ESE-detected EPR spectrum of the diluted solution (Figure 1e), weak satellites are clearly visible at the wings of the spectrum of monomer (1), which result from the hyperfine interactions of the unpaired electron with ^{47}Ti (I=5/2, natural abundance 7.44%) and ^{49}Ti (I=7/2, natural abundance 5.41%) isotopes. Due to the nearly identical g_n of the two isotopes the inner six lines of the two isotopomers are superimposed as indicated by the stick diagram in Figure 1e. A better resolution of the Ti hyperfine features was obtained on recording the X-band ESE-detected EPR spectrum with a longer inter pulse delay[19], allowing for the detailed determination of the hyperfine coupling constants via computer simulation (Figure 1S in ESI). The ^{47}Ti hyperfine coupling is dominated by a large tensor component of |77.5±0.5| MHz and two smaller components of |11±3| MHz and |18±3| MHz (footnote in Table 1). This is consistent with the results of DFT calculations reported in the following and with the principal

values of the ^{47}Ti hyperfine matrix (64.54, 11.57, 33.34 MHz) reported from a single crystal ENDOR study of Ti^{3+} in TiO_2.[20] Taking the signs to be positive as indicated by DFT calculations (*vide infra*), an a_{iso} value of 35.5±2 MHz is derived, in line with literature values reported by other Authors for Ti^{3+} molecular systems.[21,22,23]

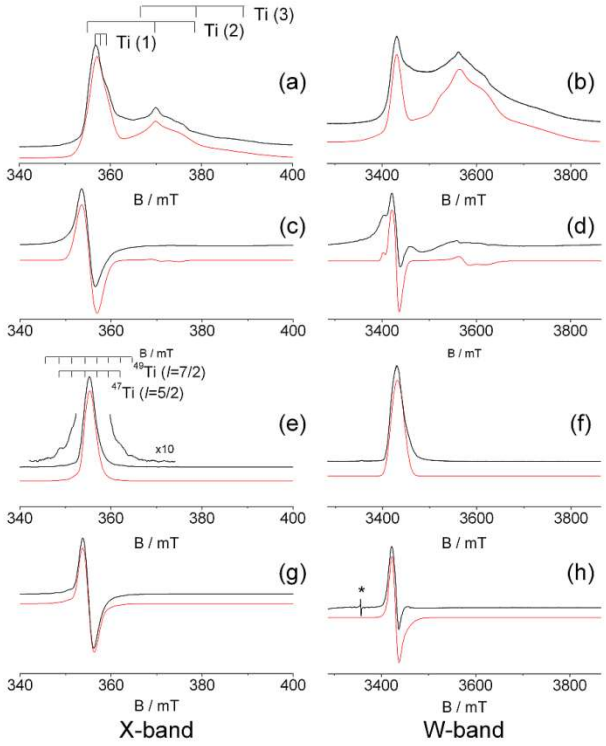

Figure 1. Experimental (black lines) and computer-simulated (red lines) CW and ESE-detected EPR spectra of frozen solutions of $TiCl_3$ in 1-methyl imidazole recorded at X- (left) and W-band (right) frequencies. Spectra (a-d) refer to the concentrated solution, while spectra (e-h) refer to the diluted solution. The parameters extracted from the simulations are listed in Table 1. All spectra were recorded at 10 K. The asterisk in Figure 1h indicates a spurious cavity signal.

For the sake of comparison EPR spectra were recorded for a $TiCl_3(Py)_3$ complex in both solid state and frozen pyridine solution. The spectra of the green solid powder recorded at three different microwave frequencies (X-, Q- and W-band) are shown in Figure 2, along with the corresponding computer simulations. The spectra can be interpreted in terms of two *S*=1/2 overlapping species with fairly anisotropic ***g*** tensors (Table 1). Anti-ferromagnetically coupled Ti^{3+}-Ti^{3+} dimers are known to be present in the $TiCl_3(Py)_3$ complex,[24] in accordance with the unusual temperature dependence of the EPR spectrum (see Figure 2S in ESI). The observed *S*=1/2 species can thus only be due to defect states, associated with isolated Ti^{3+} centers. As it will be shown later, HYSCORE experiments provide evidence for the direct ligation of ^{14}N nuclei to these isolated Ti^{3+} centers.

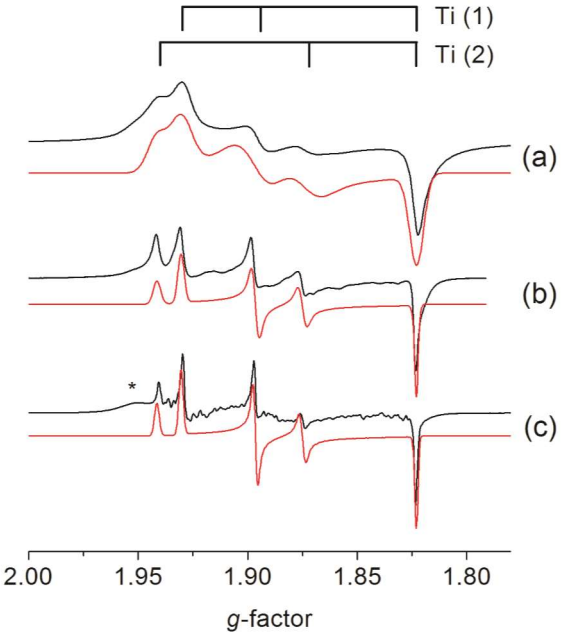

Figure 2. Experimental (black lines) and computer-simulated (red lines) CW-EPR spectra of the solid $TiCl_3(Py)_3$ complex recorded at 20 K at (a) X-band, (b) Q-band and (c) W-band frequencies. The asterisk in Figure (c) indicates a feature possibly due to S>1/2 species or to an impurity.

Dissolving the $TiCl_3(Py)_3$ complex in pyridine leads to a red colored solution. The X-band CW-EPR spectrum of the frozen solution (Figure 3) is characterized by a sharp resonance absorption at $g \approx 1.96$ with nearly isotropic symmetry, similar to the one observed for methyl-imidazole solutions (Figure 1A). In this case, however, in addition to the sharp line a broad signal is observed in the region 250 - 450 mT accompanied by a low-field component (≈166 mT), whose intensity increases with the concentration of the solution (as in the case of the methyl imidazole solution, the concentration range considered is [C] ≈ 0.02 - 0.2 M). Both these additional spectral components are characteristic of triplet states $S=1$ arising from the magnetic dipole-dipole coupling between Ti^{3+} ions in dimeric species, being the low-field and the mid-field components ascribable respectively to $\Delta M_S=\pm 2$ and $\Delta M_S=\pm 1$ transitions. Evidence for the presence of Ti^{3+} dimers in pyridine solution of $TiCl_3$ was already obtained by Carr and Smith.[24] The spectral features associated with the dimers are found to decrease by diluting the solution, indicating that the interaction between Ti^{3+} ion pairs forming dimeric species is relatively weak. From computer simulation of the spectral features associated to the dimers we extracted a zero-field splitting term $D \approx 1800$ MHz, which in the approximation of point dipole interaction corresponds to an inter-nuclear distance $r_{Ti\text{-}Ti}$ between the Ti^{3+} ions of ≈ 3.07 Å. In ref. 24 a distance $r_{Ti\text{-}Ti} \approx 3.6$ Å was calculated for dimeric Ti^{3+}-chloride species in pyridine frozen solution, which were assigned to Ti^{3+} pairs sharing two chloride ions. X-ray crystallographic studies reported a $r_{Ti\text{-}Ti}$ distance of 3.12 Å for the anion $Ti_2Cl_9^{3-}$ in which sharing of three chloride ions occurs.[25] The poor resolution of the spectrum associated to the $S=1$ state does not allow for a more detailed description of the Ti^{3+} dimers, we limit ourselves therefore to verify the consistency of these results with previous literature reports.[24] The spin-Hamiltonian parameters relative to the monomeric species ($S=1/2$), extracted from simulation of the CW-EPR spectra of the examined solutions, are also compatible with reports relative to monomeric species observed for $TiCl_3$ solutions[17] or Ti^{3+}-pyridine complexes supported on solid $MgCl_2$.[17,26]

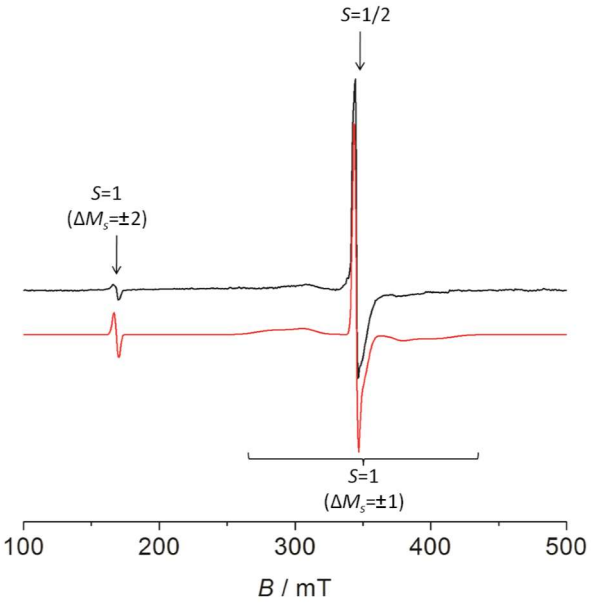

Figure 3. Experimental (black line) and simulated (red line) X-band CW EPR spectrum of a concentrated $TiCl_3(Py)_3$/pyridine frozen solution recorded at 77 K. The simulation is obtained considering the contribution of a monomeric (30%) and a dimeric (70%) Ti^{3+} species. The spin Hamiltonian parameters employed for the simulation are listed in Table 1.

The nature of the metal-ligand interaction involving the nitrogen-containing Lewis bases is of particular interest in view of the role played by nitrogen-containing ancillary ligands in both homogeneous and heterogeneous catalysts. In the following, we will thus concentrate on the monomeric species and in particular on the metal-ligand interaction as revealed by HYSCORE spectroscopy resolving ^{14}N hyperfine interactions in the different cases under study.

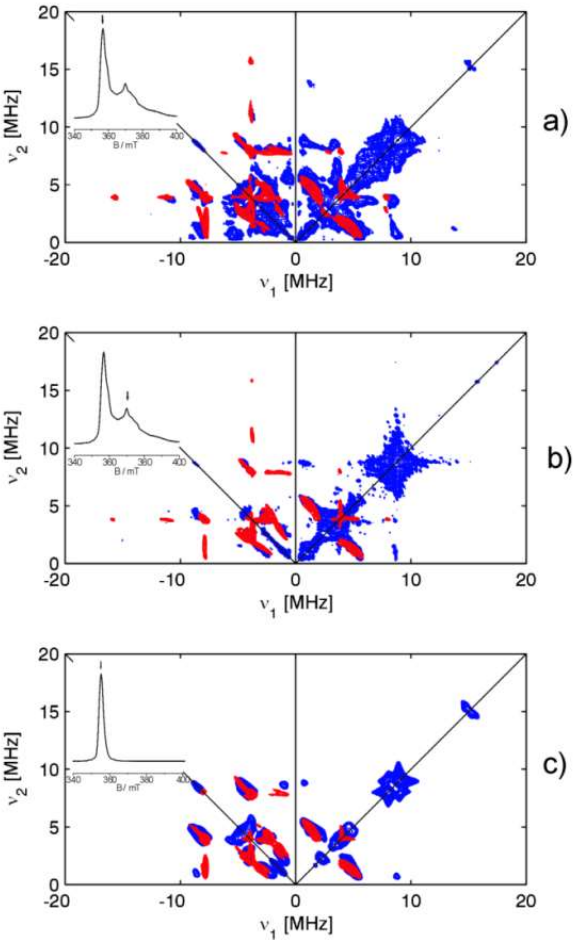

Figure 4. Experimental (blue lines) and computer-simulated (red lines) ^{14}N HYSCORE spectra of frozen solutions of $TiCl_3$ in 1-methyl imidazole recorded at X-band (ν_{mw} = 9.74 GHz). Spectra (a) and (b) refer to the concentrated solution, while spectrum (c) to the diluted solution. The spectra are taken at the observer positions (a), (c) B= 355.0 mT and (b) B_0 = 369.7 mT, corresponding to the arrows in the ESE-detected spectra in the insets. All the spectra are recorded at T = 10 K and τ value 120 ns. The spin Hamiltonian parameters extracted from the computer simulations are listed in Table 2.

Figure 4 shows the X-band HYSCORE spectra of frozen solutions of $TiCl_3$ in 1-methyl imidazole for both the low and high concentration case. The HYSCORE spectra are dominated by a pair of cross peaks centered at about (-4.6, 8.6) MHz and (-8.6, 4.6) MHz, which are assigned to the double-quantum (DQ) transitions arising from the hyperfine interaction of the unpaired electron with a ^{14}N nucleus (I = 1). In the case of the concentrated solution (Figure 4a and 4b), HYSCORE spectra recorded at a field position corresponding to the broad and narrow absorption components show the same spectral pattern indicating that both species are characterized by the presence of directly coordinated nitrogen nuclei. On lowering the contour level (Figure 3S in ESI) combination peaks of the form ($-2\nu_\beta^{DQ}$, $2\nu_\alpha^{DQ}$) are observed, which indicates that at least two nitrogen nuclei are coordinated to the Ti^{3+} ions. The HYSCORE spectrum can be satisfactory simulated considering two magnetically nearly equivalent ^{14}N nuclei. The same spin Hamiltonian parameters were used to fit the corresponding ^{14}N ENDOR spectrum (Figure 4S in ESI) confirming the validity of the spin Hamiltonian parameters. The isotropic hyperfine couplings $|a_{iso}|$ = 5.7 MHz and 6.1 MHz, derived from the simulation for the two ^{14}N nuclei, correspond to a spin density population in the N 2*s* orbital (a_0= 1540 MHz)[27] of 0.37-0.40%.

Table 1. Spin-Hamiltonian parameters derived from CW EPR simulations of Ti^{3+} monomeric species in 1-methyl imidazole and pyridine frozen solutions. The D values are in MHz units.

System		g_1	g_2	g_3	D	E/D	Ref.
$TiCl_3$ in 1-methyl imidazole	Monomer (1)[a]	1.950 ± 0.008	1.957 ± 0.008	1.966 ± 0.003	/	/	This work
	Monomer (2)	1.848 ± 0.005	1.886 ± 0.005	1.975 ± 0.003	/	/	
	Monomer (3)	1.78 ± 0.05	1.85 ± 0.03	1.91 ± 0.03	/	/	
$TiCl_3(Py)_3$ in pyridine	Monomer	1.96 ± 0.01	1.96 ± 0.01	1.92 ± 0.02	/	/	This work
	Dimer	1.96 ± 0.02	1.96 ± 0.02	1.96 ± 0.02	1800 ± 200	0.2 ± 0.1	
$TiCl_3(Py)_3$ solid state	Monomer (1)	1.823 ± 0.002	1.8965 ± 0.0005	1.9305 ± 0.0005	/	/	This work
	Monomer (2)	1.823 ± 0.002	1.8750 ± 0.0005	1.9415 ± 0.0005	/	/	
$TiCl_3(Py)_3$ in pyridine	Monomer	1.86	1.89	1.95	/	/	24
$TiCl_3$ in pyridine	Monomer	1.96	1.96	1.96	/	/	
	Dimer	2.04	1.96	1.96	1281	-	
$TiCl_3 \cdot n$DBE in pyridine	Monomer	1.960	1.960	1.960	/	/	17

a The ^{47}Ti hyperfine interaction tensor determined for this species is $\boldsymbol{A}$=[16 ±2, 77.5 ±0.5, 11±2] MHz.

Table 2. Spin-Hamiltonian parameters of the ^{14}N nuclei directly coordinated to Ti^{3+} in the centers under study in comparison to reported Ti^{3+} systems. Hyperfine and quadrupole values are given in MHz. The Euler angles α, β, γ (given in degrees) define the passive rotation of the hyperfine and quadrupole principal axes system into the ***g***-matrix principal axes system, $\boldsymbol{A}=\mathbf{R}(\alpha, \beta, \gamma)\, \boldsymbol{A}_{diagonal}\mathbf{R}^{+}(\alpha,\beta,\gamma)$.

System		$\lvert A_1 \rvert$	$\lvert A_2 \rvert$	$\lvert A_3 \rvert$	α,β,γ	$\lvert e^2qQ/h \rvert$	η	α',β',γ'	Ref.
$TiCl_3$/1-MeIm	N1	5.0 ± 0.5	5.2 ± 0.5	7.0 ± 0.2	(0,65,0) ± 10	2.7 ± 0.3	0.6 ± 0.2	(0,0,0) ± 10	This work
	N2	5.0 ± 0.5	5.2 ± 0.5	8.2 ± 0.5	(0,50,0) ± 10	2.7 ± 0.3	0.5 ± 0.2	(0,90,0) ± 20	
$TiCl_3$/Py	N1	4.6 ± 0.5	4.5 ± 0.5	5.3 ± 0.5	(0,0,0) ± 10	3.0 ± 0.3	0.05 ± 0.1	(0,-90,-10) ± 10	This work
	N2	7.1 ± 0.5	5.0 ± 0.5	5.3 ± 0.5	(0,20,60) ± 10	3.0 ± 0.3	0.05 ± 0.1	(0,30,0) ± 10	
$TiCl_3(Py)_3$solid	N1	4.6 ± 0.5	4.5 ± 0.5	5.5± 0.5	(0,70,0) ± 10	3.0 ± 0.3	0.05 ± 0.1	(0,80,90) ± 10	This work
	N2	5.3± 0.5	5.0 ± 0.5	7.1± 0.5	(0,-50,40) ± 10	3.0 ± 0.3	0.05 ± 0.1	(0,10,80) ± 10	
Ti^{3+} complex[a]		3.5 ± 0.2	3.5 ± 0.2	6.2 ± 0.2	(0,90,0) ± 20	2.3 ± 0.1	0.9 ± 0.1	-	28
TiAlPO[b]		3.5± 0.2	3.9± 0.2	4.8± 0.2	0,90,30	2.8	0.1	(0,40,60)	29
TS-1		3.4 ± 0.2	4.6 ± 0.2	5.8 ± 0.2	(0,80,20) ± 10	2.7 ± 0.2	0.1 ± 0.1	(0,10,30) ± 10	30

a [1-{2-(tert-Butyl)-2-sila-2,2-dimethyl}-2,3,4,5-tetramethylcyclopentadienyl]methyl titanium(III) complex.

b Two equivalent N nuclei.

Table 3. DFT-computed ^{14}N and ^{35}Cl hyperfine tensors for model complexes. For the 1-methyl imidazole complexes only the couplings to directly coordinated nitrogens are listed, the spin density repartition over the remote nitrogen being negligible. All couplings are given in MHz, the Euler angles are given in degrees.

Model		A_x	A_y	A_z	α,β,γ	e^2qQ/h	η	α',β',γ'
(a) $[Ti(1\text{-}MeIm)_6]^{3+}$	Ti	19.33	67.92	14.91	-12.9, 9.1, -76.2	67.95	0.042	6.6, 34.2, 85.5
	N1	-6.26	-5.98	-6.93	1.0, 65.7, -1.5	-2.06	0.957	0.3, 58.2, -0.6
	N2	-5.55	-5.09	-4.80	-0.1, 50.3, 2.0	-2.04	0.994	-0.7, 47.8, 2.3
	N3	-6.19	-5.89	-6.88	-2.5, 60.2, 4.5	-2.08	0.934	-2.9, 53.3, 4.5
	N4	-4.51	-5.49	-4.94	1.2, 28.6, -1.7	-2.03	0.964	-0.7, 45.9, -0.6
	N5	-4.36	-5.25	-4.75	-3.1, 34.3, 4.4	-2.07	0.911	-1.9, 46.4, 3.7
	N6	-5.56	-5.08	-4.77	-5.0, 50.6, 2.6	2.03	0.980	-3.7, 47.7, 1.7
(b) $[Ti(1\text{-}MeIm)_4Cl_2]^{+}$	Ti	22.08	22.62	65.62	36.5, 7.4, 48.7	70.32	0.002	35.4, 6.6, 48.8
	N1	-6.62	-5.38	-5.76	-18.1, 16.0, -31.8	-2.20	0.771	-17.3, 15.3, -32.1
	N2	-6.63	-5.36	-5.75	2.1, 18.2, 39.7	-2.20	0.770	-0.1, 17.7, 41.6
	N3	-5.77	-5.40	-6.62	-1.4, 75.9, 42.5	-2.20	0.774	-1.1, 77.0, 41.9
	N4	-5.76	-5.38	-6.63	-2.4, 73.5, -48.3	-2.20	0.772	-3.6, 74.1, -47.9
	Cl1	-1.59	-1.67	-2.77	-19.1, 4.8, 47.0	-12.91	0.055	22.7, 3.9, 50.3
	Cl2	-1.70	-1.56	-2.78	-7.4, 4.9, 55.6	-12.91	0.054	-40.5, 3.9, 48.4
(c) $[Ti(Py)_6]^{3+}$	Ti	19.62	68.73	12.22	6.2, 6.5, 64.1	76.97	0.154	6.4, 5.6, 61.8
	N1	-4.64	-5.26	-4.48	40.4, 71.3, -6.9	-2.39	0.320	44.0, 40.9, -28.0
	N2	-7.39	-5.86	-5.81	-2.3, 75.3, -7.7	-2.47	0.271	1.5, 80.7, -20.9
	N3	-5.80	-5.85	-7.38	19.0, 14.4, -25.0	-2.47	0.270	10.9, 9.1, -31.6
	N4	-5.18	-4.44	-4.61	29.5, 42.1, 62.4	-2.39	0.320	-28.9, 61.3, 23.8
	N5	-4.59	-4.42	-5.20	25.5, 51.3, 41.0	-2.39	0.335	-32.3, 64.9, 39.6
	N6	-5.23	-4.45	-4.65	-22.3, 39.9, 72.4	-2.39	0.333	-36.0, 40.8, -19.5
(d) $[Ti(Py)_4Cl_2]^{+}$	Ti	64.45	19.18	19.20	-0.1, 89.8, 15.7	50.219	0.001	0.1, 89.8, -22.2
	N1	-7.09	-5.69	-5.80	0.5, 42.1, 61.4	-2.89	0.096	-0.2, 49.8, 62.2
	N2	-5.79	-5.68	-7.09	0.1, 48.3, -27.9	-2.89	0.096	0.0, 40.5, -28.0
	N3	-7.08	-5.68	-5.79	0.5, 42.0, -28.6	-2.89	0.095	0.0, 49.5, -28.1
	N4	-5.80	-5.69	-7.10	-0.7, 48.2, 62.2	-2.89	0.096	-0.2, 40.3, 62.1
	Cl1	-1.78	-1.78	-2.63	0.2, 89.7, -37.2	-12.30	0.001	0.1, 89.8, -37.0
	Cl2	-1.79	-1.79	-2.63	-0.5, 90.0, 43.2	-12.27	0.002	0.2, 89.8, -27.1

A similar situation holds for the case of $TiCl_3(Py)_3$ complexes in both solid state and frozen solutions. In Figure 5 the Q-band HYSCORE spectra for the solid state sample and for the $TiCl_3(Py)_3$ complex dissolved in pyridine are reported along with the corresponding computer simulations. Under the experimental conditions only the *S*=1/2 species are contributing to the HYSCORE spectrum in both cases. The spin-Hamiltonian parameters extracted from the simulation compare well with those extracted from the case of the 1-methyl imidazole Ti^{3+} complex. In both cases the ^{14}N hyperfine couplings are slightly higher than those reported

for amino nitrogens axially ligated to Ti^{3+} in the [1-{2-(*t*-butyl)-2-sila-2,2-dimethyl}-2,3,4,5-tetramethylcyclopentadienyl]-methyl titanium (III) complex.[28] Similar values were also reported by some of us for coordination of ammonia to framework Ti^{3+} ions in alumino-phosphates[29] and silica porous frameworks.[30] The spin-Hamiltonian parameters reported in Table 2 thus represent the fingerprint for nitrogen ligands directly coordinated to Ti^{3+}centers in pseudo-octahedral coordination.

No clear evidence of the presence of coordinated $^{35,37}Cl$ nuclei emerges from the HYSCORE spectra of the examined solutions; however this may be due to the overwhelming intensity of the ^{14}N transitions and associated suppression effects.[31] This shortcoming can be overcome by W-band EDNMR spectroscopy. Experiments performed on the $TiCl_3(Py)_3$ solid-state complex indeed showed two sets of contributions. On the one hand, they revealed the expected peaks ascribable to coordinated ^{14}N nuclei, which can be fitted with the same spin-Hamiltonian parameters extracted from the corresponding ^{14}N HYSCORE spectra. On the other hand, additional signals could be linked to the presence of $^{35,37}Cl$ nuclei coordinated to Ti^{3+} (the W-band EDNMR and corresponding simulations are shown in Figure 5S and Table 1S in ESI).

Finally, the X-band ^{1}H Davies ENDOR spectrum was recorded for the case of the methyl-imidazole solution (Figure 6S in ESI) indicating the presence of ^{1}H hyperfine interactions with maximum couplings of approximately 3 MHz, in line with DFT calculated values (*vide infra*).

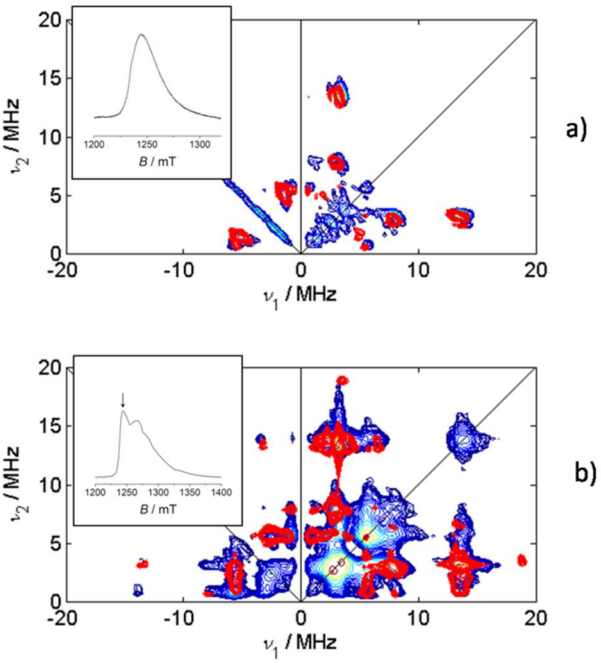

Figure 5. Experimental (blue line) and simulated (red line) Q-band HYSCORE spectra of a) a frozen solution of $TiCl_3(py)_3$ dissolved in pyridine and b) solid-state $TiCl_3(Py)_3$ complex. The spectra were recorded at τ = 260 ns and observer positions indicated by the arrows in the ESE-detected spectra shown in the inset. The parameters extracted from the computer simulation are listed in Table 2. In the case of the solid-state system, HYSCORE spectra taken at other magnetic field settings are reported in Figure 7S in ESI.

DFT models

To rationalize the HYSCORE data, DFT geometry optimized structures for a representative selection of Ti^{3+} complexes (Figure 6) were used to determine the theoretical principal hyperfine values of the relevant nuclei of the coordinated ligands. In particular we were interested in comparing the ^{14}N computed values for complexes with different ratios of directly coordinated Cl and N nuclei. Since the contributions of the $^{35,37}Cl$ nuclei seem to be suppressed in the experimental HYSCORE spectra, it is important to understand if and how the ^{14}N *hfi* couplings are influenced by the presence of directly coordinated chlorine ions. In Table 3 the computed ^{14}N hyperfine and quadrupole tensors for the complexes shown in Figure 6 are reported.

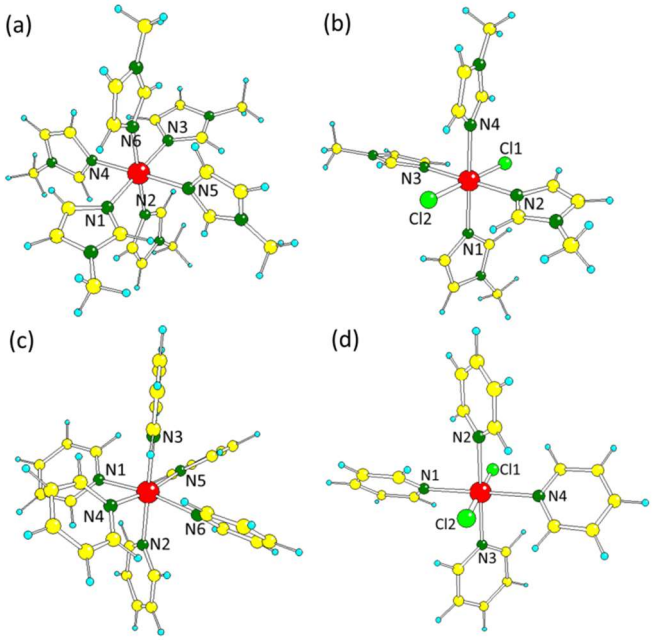

Figure 6. Geometry optimized structures employed for the computation of the hyperfine parameters listed in Table 3: (a) $[Ti(1\text{-}MeIm)_6]^{3+}$, (b) $[Ti(1\text{-}MeIm)_4Cl_2]^{+}$, (c) $[Ti(Py)_6]^{3+}$, (d) $[Ti(Py)_4Cl_2]^{+}$. The coordinates of the complexes are given as ESI.

For all complexes the ^{14}N hyperfine tensor is dominated by the isotropic contact term, which ranges between 6.4 MHz and 4.7 MHz for all nitrogens in the different complexes. Examination of Table 3 shows that the presence of coordinated chlorine ions does not alter significantly the ^{14}N couplings, which tend to be similar in the different complexes and in good agreement with the experimentally observed values. The negative sign of a_{iso} can be rationalized considering a dominant role of π-bonding interaction in the metal-ligand bonding. This is analogous to what was found for oxygen coordination in the Ti^{3+} esaquo complex.[32] The computed nuclear quadrupole couplings lie in the range ≈2-3 MHz with slightly higher values for the pyridine complexes, in line with the experimental findings (Table 2). The computed *A* values for coordinated chlorine ions are found to be strongly dependent on the coordination geometry. For the two complexes reported in Figure 6b and 6d, the values are relatively small (Table 3). This can be understood considering that the two chlorines, in this geometrical configuration, lie perpendicular to the plane where the spin density is confined (Figure 8Sa in ESI). When three coordinated chlorine ions are considered, larger values are computed for the chlorine ion in the spin density plane (Figure 8Sb in ESI) in line with the experimental values obtained from W-band ELDOR detected NMR experiments for the solid state $TiCl_3Py_3$ complex and consistent with values reported by us in previous studies on Ti^{3+} systems featuring Ti-Cl bonds.[5,6] Computed ^{1}H hyperfine couplings of the imidazole and pyridine ring protons (Table 2S in ESI) are found to have maximum values of the order of 3.5 MHz in good agreement with the experimental values observed by ENDOR which range in the interval 3.1-0.7 MHz (Figure 6S in ESI). Finally the ^{47}Ti computed hyperfine couplings (Table 3) reproduce with good accuracy the experimental values observed for monomer 1 of the methyl imidazole solution (Table 1). These values are consistent with hyperfine couplings observed in different Ti^{3+} compounds featuring distorted octahedral coordination.
The computed *g* values for the different complexes (Table 3S in ESI) are in less good agreement with the experiments. In particular, for none of the considered complexes it was possible to reproduce the reduction in the ***g*** tensor anisotropy observed experimentally for the diluted solutions. In a previous work[6] we demonstrated that directly coordinated OH^- groups formed by hydrolysis in water solutions lead to a consistent reduction in the *g* anisotropy. We could confirm this effect also theoretically in the case of nitrogen-based complexes, however the presence of coordinated OH^- groups leads to hyperfine ^{1}H couplings much larger than what experimentally observed (see Table 4S and 2S in ESI). This, together with the anhydrous conditions adopted in the experiments, excludes that OH^- coordination can be the origin for the reduction in *g* anisotropy experimentally observed here. DFT methods usually perform bad in reproducing *g* values of transition-metal complexes.[33] In addition, a recent study by Jensen and co-workers revealed a significant influence of the used functional on the accuracy of DFT-optimized geometry of organotitanium complexes, which will also influence the ***g***-tensor computation.[34] Even though we do not have at this point a conclusive explanation for the experimentally observed reduction of the ***g*** anisotropy, it seems clear that calculation of the ***g*** tensor for these complexes is very delicate and care should be taken in extrapolating general conclusions.

Conclusions

The structure and magnetic properties of Ti^{3+}-chloro complexes featuring coordinated nitrogen-containing ligands in both frozen solutions and solid state were studied by different EPR techniques assisted by DFT calculations. The full set of hyperfine and nuclear quadrupole tensors was obtained for the different systems. The ^{14}N hyperfine interaction is found to be dominated by the Fermi

contact term, showing little variation across the different complexes and in line with values reported for different systems featuring the direct coordination of nitrogen Lewis bases to Ti^{3+} ions. The reported values can therefore be considered as diagnostic of direct nitrogen coordination to Ti^{3+} and will be useful in the assessment of the nature and role of nitrogen containing Lewis bases in more complex systems such as heterogeneous Ziegler-Natta catalysts.

Acknowledgements

This work is part of the research program of the Dutch Polymer Institute (DPI), project nr. 754. We gratefully acknowledge Prof. M. Terano for providing the $TiCl_3py_3$ complex and Prof. V. Busico for several useful discussions.

Notes and references

1 G. Natta, P. Corradini, G. Allegra, *J. Polym. Sci.,* 1961, **51**, 399.
2 P. Sobota, K. Przybylak, J. Utko, L. B. Jerzykiewicz, A. J. L. Pombeiro, M. F. C. Guedes da Silva, K. Szczegot, *Chem. Eur. J.,* 2001, **7**, 951.
3 J. Pinkas, R. Gyepes, I. Císařová, J. Kubišta, M. Horáček, K. Mach, *Organomet*., 2014, **33**, 3399.
4 A. Cangönül, M. Behlendorf, A. Gansäuer, M. Van Gastel, *Inorg. Chem*., 2013, **52**, 11859.
5 E. Morra, E. Giamello, S. Van Doorslaer, G. Antinucci, M. D'Amore, V. Busico, M. Chiesa, *Angew. Chem. Int. Ed.*, 2015, **54**, 4857.
6 S. Maurelli, E. Morra, S. Van Doorslaer, V. Busico, M. Chiesa, *Phys. Chem. Chem. Phys.*, 2014, **16**, 19625.
7 P. Höfer, A. Grupp, H. Nebenführ, M. Mehring, *Chem. Phys. Lett.*, 1986, **132**, 279.
8 P. M. Schosseler, T. Wacker, A. Schweiger, *Chem. Phys. Lett.*, 1994, **224**, 319.
9 S. Stoll, A. Schweiger, *J. Magn.Reson.*, 2006, **178**, 42.
10 F. Neese, *J. Chem. Phys.*, 2001, **115**, 11080; F. Neese, *J. Phys. Chem. A*, 2001, **105**, 4290; F. Neese, *J. Chem. Phys.*, 2003, **118**, 3939; F. Neese, *J. Chem. Phys.,* 2005, **122**, 034107/1.
11 J. P. Perdew, *Phys. Rev. B: Condens. Matter Mater. Phys*,. 1986, **33**, 8822; J. P. Perdew, *Phys. Rev. B: Condens. Matter Mater. Phys.*, 1986, **34**, 7406; A. D. Becke, *Phys. Rev. A: At., Mol., Opt. Phys*., 1988, **38**, 3098.
12 The Ahlrichs (2df,2pd) polarization functions were obtained from the TurboMole basis set library under ftp.chemie.uni-karlsruhe.de/pub/basen, R. Ahlrichs and co-workers, unpublished.
13 A. Schäfer, H. Horn, R. Ahlrichs, *J. Chem. Phys.*, 1992, **97**, 2571.
14 V. Barone in *Recent Advances in Density Functional Methods*, ed. D. P. Chong, World Scientific Publ. Co. (Singapore), 1996, p. 287.
15 A. Gansäuer, M. Behlendorf, A. Cangönül, C. Kube, J. M. Cuerva, J. Friedrich, M. van Gastel, *Angew. Chem. Int. Ed.*, 2012, **51**, 3266.
16 S. Sinnecker, A. Rajendran, A. Klamt, M. Diedenhofen and F. Neese, *J. Phys. Chem. A*, 2006, **110**, 2235.
17 A. A. Tregubov, V. A. Zakharov, T. B. Mikenas, *J. Polym. Sci. A Polym. Chem.,* 2009, **47**, 6362.
18 V. A. Poluboyarov, V. F. Anufrienko, V. A. Zakharov, S. A. Sergeev, S. I. Makhtarulin, G. D. Bukatov, *React. Kinet. Catal. Lett.*, 1984, **26**, 347.
19 A. Schweiger, G. Jeschke in *Principles of Pulse Paramagnetic Resonance*, Oxford University Press (Oxford, UK) 2001, ch. 8 p. 214.
20 A. T. Brant, N. C. Giles, S. Yang, M. A. R. Sarker, S. Watauchi, M. Nagao, I. Tanaka, D. A. Tryk, A. Manivannan, L. E. Halliburton, *J. Appl. Phys.*, 2013, **114**, 113702.
21 J. B. Raynor, A. W. L. Ball, *Inorg. Chim. Acta*, 1973, **7**, 315.
22 E. L. Waters, A. H. Maki, *Phys. Rev.*, 1962, **125**, 233.
23 M. Haehnel, J. B. Priebe, J. C.-H. Yim, A. Spannenberg, A. Brückner, L. L. Schafer, U. Rosenthal, *Chem. Eur. J.*, 2014, **20**, 7752.
24 S. G. Carr, T. D. Smith, *J. Chem*. Soc., *Dalton Trans.,* 1972, 1887.
25 G. J. Wessel, D. J. Ijdo, *Acta Cryst.,* 1957, **10**, 466.
26 H. Mori, K. Hasebe, M. Terano, *Polymer,* 1999, **40**, 1389.
27 J. A. J. Fitzpatrick, F. R. Manby, C. M. Western, *J. Chem. Phys*., 2005, **122**, 084312-1.
28 S. Van Doorslaer, J. J. Shane, S. Stoll, A. Schweiger, M. Kranenburg, R. J. Meier, *J. Organomet. Chem*., 2001, **634**, 185.
29 S. Maurelli, V. Muthusamy, M. Chiesa, G. Berlier, S. Van Doorslaer, *J. Am. Chem. Soc.,* 2011, **133**, 7340.
30 E. Morra, E. Giamello, M. Chiesa, *Chem. Eu. J.,* 2014, **20**, 7381.
31 S. Stoll, C. Calle, G. Mitrikas, A. Schweiger, *J. Magn. Reson.,* 2005, **177**, 93.
32 S. Maurelli, S. Livraghi, M. Chiesa, E. Giamello S. Van Doorslaer, C. Di Valentin, G. Pacchioni, *Inorg. Chem.*, 2011, **50**, 2385.
33 M. Orio, D. A. Pantazis, F. Neese, *Photosynth. Res*., 2009, **102**, 443.
34 Y. Minenkov, A. Singstad, G. Occhipinti, V. R. Jensen, *Dalton Trans.*, 2012, **41**, 5526.